Progress in Nuclear Magnetic Resonance Spectroscopy 96 (2016) 47–57

Contents lists available at ScienceDirect

Progress in Nuclear Magnetic Resonance Spectroscopy

journal homepage: www.elsevier.com/locate/pnmrs

Quantitative analysis of protein–ligand interactions by NMR

Ayako Furukawa [a,b], Tsuyoshi Konuma [a,c], Saeko Yanaka [a,d], Kenji Sugase [a,e,*]

[a] Bioorganic Research Institute, Suntory Foundation for Life Sciences, 1-1-1 Wakayamadai, Shimamoto, Mishima, Osaka 618-8503, Japan
[b] Graduate School of Medical Life Science, Yokohama City University, 1-7-29 Suehiro-cho, Tsurumi-ku, Yokohama 230-0045, Japan
[c] Department of Structural and Chemical Biology, Icahn School of Medicine at Mount Sinai, New York, NY 10029, USA
[d] Department of Life and Coordination-Complex Molecular Science, Biomolecular Functions, Institute of Molecular Science, National Institute of Natural Sciences, Japan
[e] Department of Molecular Engineering, Graduate School of Engineering, Kyoto University, Kyoto-Daigaku Katsura, Nishikyo-Ku, Kyoto 615-8510, Japan

Edited by David Neuhaus and Beat Meier

ARTICLE INFO

Article history:
Received 19 November 2015
Accepted 21 February 2016
Available online 3 March 2016

Keywords:
Protein–ligand interaction
Relaxation
Chemical exchange
Chemical shift timescale
Kinetics

ABSTRACT

Protein–ligand interactions have been commonly studied through static structures of the protein–ligand complex. Recently, however, there has been increasing interest in investigating the dynamics of protein–ligand interactions both for fundamental understanding of the underlying mechanisms and for drug development. NMR is a versatile and powerful tool, especially because it provides site-specific quantitative information. NMR has widely been used to determine the dissociation constant (K_D), in particular, for relatively weak interactions. The simplest NMR method is a chemical-shift titration experiment, in which the chemical-shift changes of a protein in response to ligand titration are measured. There are other quantitative NMR methods, but they mostly apply only to interactions in the fast-exchange regime. These methods derive the dissociation constant from population-averaged NMR quantities of the free and bound states of a protein or ligand. In contrast, the recent advent of new relaxation-based experiments, including R_2 relaxation dispersion and ZZ-exchange, has enabled us to obtain kinetic information on protein–ligand interactions in the intermediate- and slow-exchange regimes. Based on R_2 dispersion or ZZ-exchange, methods that can determine the association rate, k_{on}, dissociation rate, k_{off}, and K_D have been developed. In these approaches, R_2 dispersion or ZZ-exchange curves are measured for multiple samples with different protein and/or ligand concentration ratios, and the relaxation data are fitted to theoretical kinetic models. It is critical to choose an appropriate kinetic model, such as the two- or three-state exchange model, to derive the correct kinetic information. The R_2 dispersion and ZZ-exchange methods are suitable for the analysis of protein–ligand interactions with a micromolar or sub-micromolar dissociation constant but not for very weak interactions, which are typical in very fast exchange. This contrasts with the NMR methods that are used to analyze population-averaged NMR quantities. Essentially, to apply NMR successfully, both the type of experiment and equation to fit the data must be carefully and specifically chosen for the protein–ligand interaction under analysis. In this review, we first explain the exchange regimes and kinetic models of protein–ligand interactions, and then describe the NMR methods that quantitatively analyze these specific interactions.

Contents

* Corresponding author at: Department of Molecular Engineering, Graduate School of Engineering, Kyoto University, Kyoto-Daigaku Katsura, Nishikyo-Ku, Kyoto 615-8510, Japan. Tel.: +81 75 383 7063; fax: +81 75 383 2541.
E-mail address: sugase@moleng.kyoto-u.ac.jp (K. Sugase).

http://dx.doi.org/10.1016/j.pnmrs.2016.02.002
0079-6565/

1. Introduction

Proteins interact with various ligand molecules, such as peptides, proteins, nucleic acids, and small organic compounds, and these interactions play central roles in biological systems [1,2]. Details of such interactions (hereafter termed protein–ligand interactions) have been studied by solving structures of the protein–ligand complex using X-ray crystallography and NMR spectroscopy. The complex structures, which are determined as static pictures, provide information on site-specific interactions between a protein and a ligand molecule. If the structure of the free state of the protein is determined as well as the complex structure, the conformational changes upon ligand binding can also be understood. Such structural information is often utilized for drug development [3].

Recently, in addition to attempts to understand protein–ligand interactions from static pictures [4], there is an increasing interest in investigating the dynamic processes of protein–ligand interactions so as to improve our fundamental understanding of their mechanisms [5,6]. Protein–ligand interactions can be studied by several biophysical techniques [7], including ultraviolet/visible absorption spectroscopy [8], analytical ultracentrifugation [9], circular dichroism [10], fluorescence spectroscopy [11], differential scanning fluorimetry [12], surface plasmon resonance [13], isothermal titration calorimetry (ITC) [14], quartz crystal microbalance [15], mass spectrometry [16], small-angle X-ray scattering [17], atomic force microscopy [18], and NMR [19]. These provide information that is difficult to derive from a static structure alone—for example, kinetic parameters, thermodynamic parameters, dissociation constants, and conformational changes upon ligand binding. Among them, NMR is the most versatile and powerful tool with which to study the dynamics of protein–ligand interactions, especially because it provides site-specific quantitative information [19].

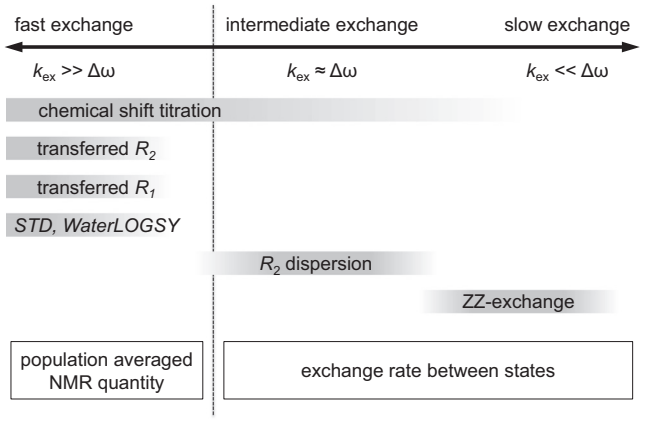

Fig. 1. NMR methods used for quantitative analysis of protein–ligand interactions. NMR methods described in the main text are shown along with the chemical shift timescales. k_{ex} denotes the exchange rate, which is defined as the sum of the forward and backward rates in units of s^{-1}: $k_{ex} = [B]k_{on} + k_{off}$. $\Delta\omega$ denotes the chemical shift deference between the free and bound states in units of rad s^{-1}.

With regard to quantitative NMR analysis of protein–ligand interactions, NMR has most widely been used to determine the dissociation constant, K_D [20,21], in particular, for relatively weak interactions (K_D > 10 μM) that would be difficult to investigate by other biophysical methods [22]. Dissociation constants are most simply determined from the chemical-shift changes of a protein in response to ligand titration [23]; this method is designated chemical-shift titration. Concomitantly, the binding site on the surface of the protein can also be roughly identified from chemical shift data because the chemical shifts of the protein are altered both by direct contact with the ligand and by its own conformational changes that occur upon ligand binding. This method is one of the simplest and earliest to be applied in this field, but it can be easily used to examine whether a ligand binds to its target protein and vice versa.

There are other quantitative NMR methods (Fig. 1), but most of them can be applied only to interactions in the fast-exchange regime (see Section 2.1). They are mainly used to derive dissociation constants, using population-averaged NMR observable quantities of the free and bound states of a protein or ligand. This type of NMR method includes the chemical-shift titration experiment, in which population-averaged chemical shifts of the free and bound states are observed during a ligand titration. In addition to chemical shift, the population-averaged longitudinal relaxation rate R_1 and transverse relaxation rate R_2 can also be used to determine dissociation constants.

By contrast, some NMR relaxation experiments, such as relaxation dispersion [24–26] and ZZ-exchange spectroscopy [27], can provide the exchange rates of a protein and are capable of analyzing interactions in the intermediate- and slow-exchange regimes. These methods have been applied to many protein–ligand interactions in order to understand their mode of action from the viewpoint of protein dynamics [28–38]. In particular there are recently developed methods that can determine the association rate, k_{on}, dissociation rate, k_{off}, and K_D [30,31,37], using R_2 relaxation dispersion or ZZ-exchange curves measured for multiple samples with different protein/ligand concentration ratios, similarly to the ligand titration experiment. The relaxation or ZZ-exchange curves obtained are then fitted to theoretical kinetic models [39]. These methods are suitable for the analysis of protein–ligand interactions with a micromolar or sub-micromolar dissociation constant, but not for very weak interactions, which are typically in very fast exchange. This contrasts with the above-mentioned quantitative NMR methods that are used to analyze population-averaged NMR quantities (Fig. 1). Therefore, it is essential to choose carefully an appropriate method for the protein–ligand interaction under analysis.

In this review, we first explain the exchange regimes and kinetic models of protein–ligand interactions in equilibrium. We then describe the NMR methods that can analyze protein–ligand interactions quantitatively, with a particular focus on relatively new methods that utilize NMR relaxation measurements and on features of the interactions that define which of the NMR methods is applicable.

2. Theoretical aspects of protein–ligand interactions

To analyze protein–ligand interactions quantitatively by NMR, an appropriate method should be carefully chosen in accordance with the chemical exchange regime of the interaction on the chemical shift timescale. Furthermore, in the case of NMR methods that deal with the kinetic rates of the interaction, an appropriate interaction model, such as a two- or three-state exchange model, must be chosen to analyze the data because—except for very slow interactions on a timescale of seconds or slower—protein–ligand interactions are difficult to analyze directly in real time by NMR [40,41]. Therefore, the collected NMR data are fitted to a theoretical equation derived for a specific interaction model after the NMR measurements have been completed. Multiple models are usually tested, and the most physiologically and statistically reasonable model is chosen by assessing both the fitting quality and the parameters obtained. In this section, we explain the chemical exchange regimes with a specific focus on protein–ligand interactions and their kinetic models.

2.1. Exchange regime

Protein–ligand interactions are schematically represented as equilibrium equations; non-equilibrium interactions such as enzyme reactions are beyond the scope of this review. Most NMR studies of protein–ligand interactions are based on a two-state exchange model:

$$\mathrm{A} + \mathrm{B} \underset{k_{\mathrm{off}}}{\overset{[\mathrm{B}]k_{\mathrm{on}}}{\rightleftharpoons}} \mathrm{A:B} \tag{1}$$

where A, B, and A:B denote the protein, ligand, and the protein–ligand complex, respectively. In typical protein NMR experiments, A is an isotope ^{15}N and/or ^{13}C-labeled protein and B is unlabeled ligand. [B] denotes the concentration of free B, which can be calculated from the total concentrations of A ($[A]_0$) and B ($[B]_0$), and the dissociation constant K_D:

$$[\mathrm{B}] = \frac{1}{2}\left\{-K_{\mathrm{D}} - [\mathrm{A}]_0 + [\mathrm{B}]_0 + \sqrt{(K_{\mathrm{D}} + [\mathrm{A}]_0 - [\mathrm{B}]_0)^2 + 4[\mathrm{B}]_0 K_{\mathrm{D}}}\right\} \tag{2}$$

$$K_{\mathrm{D}} = \frac{k_{\mathrm{off}}}{k_{\mathrm{on}}} = \frac{[\mathrm{A}][\mathrm{B}]}{[\mathrm{A:B}]} \tag{3}$$

The parameters that characterize the chemical exchange regime of a protein–ligand interaction are the exchange rate, k_{ex} (in units of s^{-1}), and the chemical-shift difference between the free and bound states, $\Delta\omega$ (in units of rad s^{-1}) [42]. $\Delta\omega$ is calculated from the chemical-shift difference in units of ppm ($\Delta\delta$) as:

$$\Delta\omega = 2\pi\Delta\delta B_0 \tag{4}$$

where B_0 denotes the magnetic field in units of Hz. For a strong interaction (K_D < 0.1 μM), the free and bound resonances of a protein are directly observed by using samples with and without ligand, respectively. For a weak interaction (K_D > 10 μM), by contrast, the observable chemical shift difference $\Delta\delta_{obs}$ at a 1:1 concentration ratio is usually smaller than the exact chemical shift difference, $\Delta\delta$, because the protein is not fully saturated by the ligand. Thus, an excess of ligand should be mixed with the protein to obtain the exact $\Delta\delta$ value. Alternatively, $\Delta\delta$ can be estimated by a chemical shift titration experiment (see Section 3.3).

In the case of the two-state exchange model (Eq. (1)), k_{ex} is defined as sum of the forward and backward rates:

$$k_{\mathrm{ex}} = [\mathrm{B}]k_{\mathrm{on}} + k_{\mathrm{off}} \tag{5}$$

Fig. 2 shows simulated NMR spectra of protein–ligand interactions at k_{ex} rates of 10^6, 10^3, and 1 s^{-1}. The population of the bound state is 0.5 in Fig. 2a–c, and 0.1 in Fig. 2d–f. Free and bound

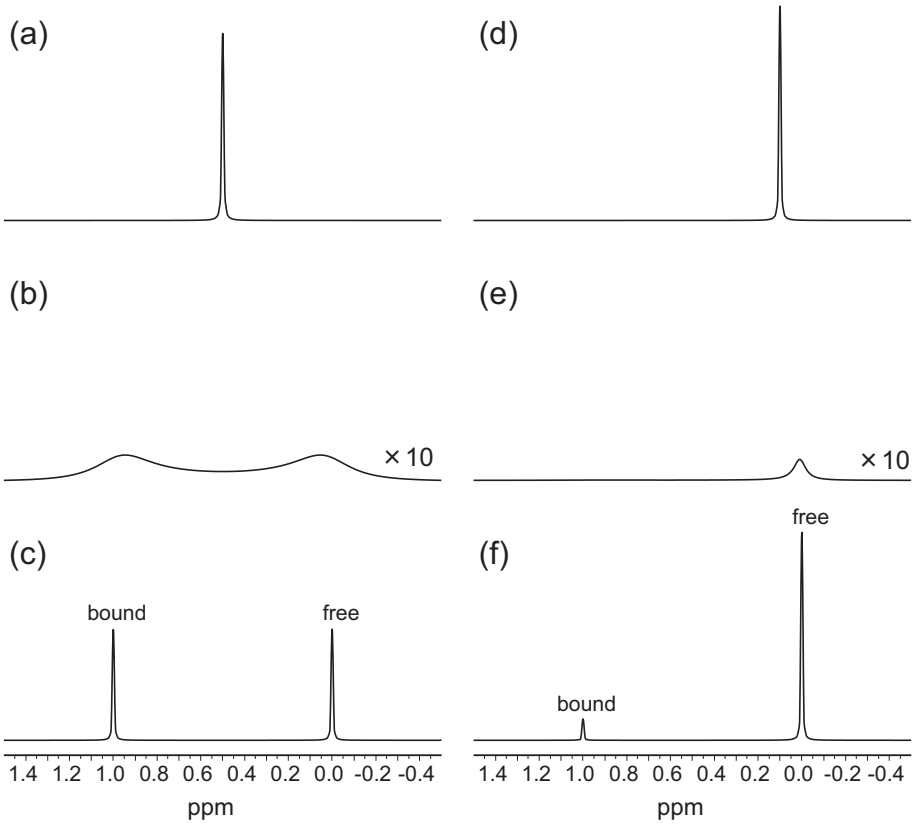

Fig. 2. Chemical exchange in a two-state exchange model. (a, d) Fast exchange, (b, e) intermediate exchange, and (c, f) slow exchange. The spectra were simulated by using $\Delta\omega$ = 3141 rad s^{-1} (1 ppm at a B_0 frequency of 500 MHz), and k_{ex} = 10^6 s^{-1} (a, d), 10^3 s^{-1} (b, e), and 1 s^{-1} (c, f). The populations of the bound states were 0.5 (a–c) and 0.1 (d–f), and the intrinsic transverse relaxation rates of the free and bound states were both set to 10 s^{-1}. The vertical direction in (b) and (e) is expanded 10-fold.

resonances appear at 0 and 1 ppm, respectively; therefore, $\Delta\omega$ is 3141 rad s^{-1} at B_0 = 500 MHz. The intrinsic relaxation rates of the free and bound resonances are both set to 10 s^{-1}.

If k_{ex} is much larger than $\Delta\omega$ ($k_{ex} \gg \Delta\omega$), the interaction is in the fast-exchange regime, and an NMR signal appears at the population-averaged chemical shift of the free and bound states (Fig. 2a and d). If k_{ex} is comparable in magnitude to $\Delta\omega$ ($k_{ex} \approx \Delta\omega$), the interaction is in the intermediate exchange regime, and the NMR signal becomes broad owing to the contribution of transverse relaxation due to chemical exchange, termed R_{ex} (Fig. 2b and e). When the population is highly skewed, as in the case where the bound population is 0.1 (Fig. 2e), the resonance of the minor state is unobservable. This often happens in titration experiments. If k_{ex} is much smaller than $\Delta\omega$ ($k_{ex} \ll \Delta\omega$), the interaction is in the slow-exchange regime, and a pair of NMR signals corresponding to the free and bound states appears at different chemical shifts (Fig. 2c and f). Provided that the relaxation rates of the free and bound resonances are identical, the signal intensities are proportional to the fraction of the corresponding states.

These classifications of the exchange regime are the same as those of chemical (conformational) exchange in a molecule, but it should be emphasized that the exchange regime of a protein–ligand interaction can change according to the concentrations of A and B. Although $\Delta\omega$ is invariant at any concentration of A and B, k_{ex} is dependent on concentration (Eqs. (2) and (5)). This property of chemical exchange must be taken into account when a protein–ligand interaction is quantitatively analyzed by NMR, especially by the chemical-shift titration experiment. In some cases, the exchange regime of the interactions can change from slow to intermediate to fast exchange during ligand titration (see Section 3.3).

2.2. Kinetic model

In the previous section, we explained the kinetics established for the two-state exchange model (Eq. (1)). In addition to the two-state exchange model, some interaction studies using NMR, especially relaxation dispersion spectroscopy, use three-state exchange models, for which four different kinetic binding models can be constructed: induced fit [43], conformational selection (pre-equilibrium) [44], forked two-site binding, and triangular two-site binding models.

$$\mathrm{A} + \mathrm{B} \underset{k_{off}}{\overset{[\mathrm{B}]k_{on}}{\rightleftarrows}} \underline{\mathrm{A:B}} \underset{k_{-1}}{\overset{k_1}{\rightleftarrows}} \mathrm{A:B} \quad \text{(induced fit)} \tag{6}$$

$$\underline{\mathrm{A}} + \mathrm{B} \underset{k_{-1}}{\overset{k_1}{\rightleftarrows}} \mathrm{A} + \mathrm{B} \underset{k_{off}}{\overset{[\mathrm{B}]k_{on}}{\rightleftarrows}} \mathrm{A:B} \quad \text{(conformational selection)} \tag{7}$$

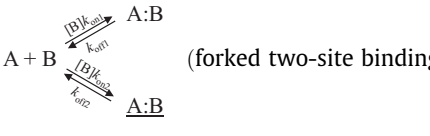

(forked two-site binding) (8)

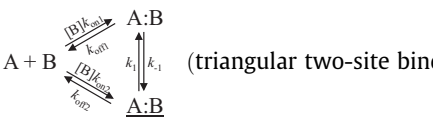

(triangular two-site binding) (9)

where underscored letters represent the states whose conformations are different from that of the other free or bound state in the same model. The induced fit model has an on-pathway binding intermediate state in-between the free and bound states (Eq. (6)). In this model, the protein adjusts its conformation to fit the shape of its binding site after the ligand binds. The conformational selection model, originally called the pre-equilibrium model, has two free states that interconvert with each other (Eq. (7)). In this model, the protein adopts a bound-like conformation before the ligand binds, and this free state then proceeds to the bound state. The forked two-site binding model has an off-pathway bound state in addition to the correct bound state (Eq. (8)), but the two bound states do not interconvert with each other. In contrast to the forked two-site binding model, the triangular two-site binding model has two bound states that do interconvert (Eq. (9)). In addition to these four models, one more three-state exchange model can theoretically be constructed; this model is the same as the conformational selection model except that both free states proceed to the same bound state. This model, however, seems physiologically unreasonable because the same bound conformation is formed from two different free conformations with no intermediate in either pathway.

Eq. (2) is valid for all the three-state exchange models, but the definitions of K_D differ from Eq. (3):

$$K_D = \frac{k_{off}}{k_{on}} \times \frac{k_{-1}}{k_1 + k_{-1}} \quad \text{(induced fit)} \tag{10}$$

$$K_D = \frac{k_{off}}{k_{on}} \times \frac{k_1 + k_{-1}}{k_1} \quad \text{(conformational selection)} \tag{11}$$

$$K_D = \frac{k_{off1} k_{off2}}{k_{on1} k_{off2} + k_{on2} k_{off1}} \quad \text{(forked two-site binding)} \tag{12}$$

$$K_D = \frac{k_{off1} k_{off2} + k_{off1} k_{-1} + k_{off2} k_1}{k_{on1}(k_{off2} + k_1 + k_{-1}) + k_{on2}(k_{off1} + k_1 + k_{-1})} \quad \text{(triangular two-site binding)} \tag{13}$$

These equations including Eq. (2) are derived by using the principle of microscopic reversibility. For example, in the case of the induced fit model, Eqs. (2) and (10) are derived by solving the following simultaneous equations:

$$\begin{cases} [\mathrm{A}][\mathrm{B}]k_{on} = [\underline{\mathrm{A:B}}]k_{off} \\ [\underline{\mathrm{A:B}}]k_1 = [\mathrm{A:B}]k_{-1} \\ [\mathrm{A}] + [\underline{\mathrm{A:B}}] + [\mathrm{A:B}] = [\mathrm{A}]_0 \\ [\mathrm{B}] + [\underline{\mathrm{A:B}}] + [\mathrm{A:B}] = [\mathrm{B}]_0 \end{cases} \tag{14}$$

3. Protein–ligand interaction in the fast-exchange regime

To quantitatively analyze protein–ligand interactions in the fast-exchange regime, saturation transfer difference (STD) [45,46] and water-ligand observed via gradient spectroscopy (WaterLOGSY) [47,48] have been widely used, in particular for drug screening. Here we only briefly explain these two NMR methods, before describing in more detail other methods based on the fact that some NMR quantities, such as the longitudinal relaxation rate R_1, transverse relaxation rate R_2, and chemical shift δ, are observed as population-averaged values of the free and bound states during fast exchange. The NMR methods that analyze population-averaged R_1, R_2, and δ are called transferred R_1 [49], transferred R_2 [50], and chemical shift titration, respectively. They have been used to determine K_D but not kinetic rates, except for some recent analyses of chemical shift titration data.

3.1. STD and WaterLOGSY

Saturation transfer difference (STD) and water-ligand observed via gradient spectroscopy (WaterLOGSY) are typically used for screening ligands that bind to a protein with K_D in the range of 10^{-3} to 10^{-8} M [51]. The samples analyzed by these NMR methods contain a ligand or a mixture of ligands in the presence of a small amount of a protein. The ^{1}H resonances of the bound ligand are perturbed, and the perturbed magnetization is transferred to the

^{1}H resonances of the free ligand via fast chemical exchange. Therefore, the NMR signals of the interaction sites on the ligand can be detected. The pathway of the magnetization transfer is different between STD and WaterLOGSY. In the case of WaterLOGSY, the ^{1}H resonance of bulk water are excited and the magnetization is transferred from transiently bound water to the bound ligand. Magnetization transfer may also occur via indirect spin diffusion through exchangeable and nonexchangeable ^{1}H of the protein. In the case of STD, a selected ^{1}H spectral region of the protein is saturated, which causes saturation of additional ^{1}H resonances of the protein via spin diffusion and magnetization transfer from the protein to the ligand via intermolecular NOEs.

Because the NMR signals of the ligand are analyzed, these methods are called ligand-based NMR techniques. In addition, because the NMR signals of the protein are not observed, the protein can be very large (>50 kDa) and does not have to be isotope-labeled. Furthermore, the amount of protein is usually not very high (micromolar range) [52]. STD and WaterLOGSY can probe weak interactions that are difficult to detect by other biophysical experiments, and the analytical samples can contain a mixture of ligands [47]; therefore, they are widely used for drug screening. The identified ligands are then optimized by using combinatorial chemistry and structure-based drug design, among other techniques [53]. Recently, Antanasijevic et al. [54] compared the sensitivities of STD and WaterLOGSY using three experimental systems: ketoprofen–bovine serum albumin, tert-butyl hydroquinone–hemagglutinin, and chloramphenicol–ribosome. The authors found that WaterLOGSY was more sensitive than STD in all three systems [54]. They attribute the higher sensitivity of WaterLOGSY to be due to simultaneous saturation of multiple sources of cross correlation, including direct NOEs of water and exchangeable groups and indirect NOEs of ^{1}H–C groups.

3.2. Transferred R_1 and transferred R_2

LaPlante et al. [49] developed the transferred R_1 method, in which relative changes in the R_1 relaxation rate of a ligand (an isotope-labeled small protein) in the free state and in the presence of a small amount of the target protein are measured. In the case of fast exchange, the longitudinal relaxation rate R_{1av} is measured as a population-averaged value of the free and bound states of the ligand:

$$R_{1av} = p_F R_{1F} + p_B R_{1B} \tag{15}$$

where p_F and p_B denote the fraction of the ligand in the free and bound states, respectively, and R_{1F} and R_{1B} are the longitudinal relaxation rates of the ligand in the free and the bound states, respectively. Note that the transferred R_1 method can be applied only if the ligand has a large difference between its R_{1F} and R_{1B} values. If R_{1F} and R_{1B} are comparable, R_{1av} does not change no matter how much protein is added to the ligand solution. Also, because the longitudinal rate R_1 decreases with increasing molecular weight, the protein that is titrated into the ligand must be much larger than the ligand in order to obtain a sufficient difference between the R_{1F} and R_{1av} rates. How much difference is required depends on the quality of the NMR data. Thus, it is a good strategy to simulate transferred R_1 profiles using R_1 values of the protein and ligand that are estimated from their molecular weights and including a certain experimental error before conducting the NMR measurements. If R_{1av} is measured for multiple samples with different protein/ligand concentration ratios and R_{1av} changes with the concentration ratio, then K_D can be derived from the following equation:

$$K_D = \frac{p_F}{p_B}([B]_0 - p_B[A]_0) \tag{16}$$

which in turn is derived from the definition of $K_D = [A][B]/[A:B]$ for the two-state exchange model (Eq. (1)). LaPlante et al. [49] applied the transferred R_1 method to BILN127SE, an inhibitor of the nonstructural 3 protease domain of the hepatitis C virus, and used variations in the R_1 values for different residues to characterize the local dynamics of the inhibitor rather than determining the K_D value.

The transferred R_2 method is similar to the transferred R_1 method (R_1 in Eq. (15) is simply replaced by R_2), but is comparatively more sensitive to protein–ligand interactions because the difference in the relaxation rate between the free and bound states is usually larger for R_2 than for R_1 [50]. In contrast to R_1, the transverse relaxation rate R_2 increases with increasing molecular weight. Note that the transferred R_2 method can be applied only if the interaction is sufficiently fast to prevent any contribution to the measured R_2 rate from chemical exchange between the free and bound states, and if the exchange rate is faster than the R_2 rate of the bound state. Using the transferred R_2 method, Su et al. [50] determined K_D for the interaction between the τ subunit of the *Escherichia coli* DNA polymerase III complex (15 kDa) and the α subunit (130 kDa).

3.3. Chemical-shift titration

Chemical-shift titration is a simple method with which to map a ligand-binding site on a target protein and estimate K_D. Typically, an unlabeled ligand, such as a small compound, protein or nucleic acid, is titrated into an isotope (^{15}N and/or ^{13}C)-labeled protein, and a 1D or 2D NMR spectrum of the protein is recorded after each ligand addition [21]. This very simple experiment has been applied to a large number of ligand–protein interactions. In the case of fast exchange, NMR signals appear at the population-averaged chemical shifts of the free and bound states, and K_D is estimated from curve fitting of the chemical shift changes as a function of the total concentrations of the protein ($[A]_0$) and the ligand ($[B]_0$) [42]:

$$\Delta\delta_{obs} = \frac{\Delta\delta_{max}}{2[A]_0}\left\{K_D + [A]_0 + [B]_0 - \sqrt{(K_D + [A]_0 + [B]_0)^2 - 4[A]_0[B]_0}\right\} \tag{17}$$

where $\Delta\delta_{max}$ is the chemical shift difference between the free and bound states in the case of slow exchange. In addition to K_D, $\Delta\delta_{max}$ is also estimated from the curve fitting. Eq. (17) is valid only when k_{off} is much larger than $\Delta\omega$ ($=2\pi\Delta\delta_{max}B_0$) because the exchange regime is always in fast exchange during the titration. It is important to treat both $[A]_0$ and $[B]_0$ as independent variables in the curve fitting to increase in the accuracy of the fitted K_D and $\Delta\delta_{max}$ values [55]. Alternatively, the application of line shape analysis to a series of NMR spectra from a titration experiment provides accurate and precise kinetic parameters of the interaction such as k_{off} [56].

For some protein–ligand interactions, the observed resonances do not move linearly during a titration but instead follow curved tracks, which might indicate the presence of at least two binding modes. Even in such cases, the titration experiment in combination with singular value analysis can provide two distinct K_D values [57,58]. However, care must be taken in analyzing the curvature of chemical-shift changes because sigmoidal-like curvature can be observed even for the simplest single-binding interaction represented in Eq. (1) (Fig. 3). The singular value analysis is valid only for cases where the exchange regimes of all binding modes in the interaction are always in fast exchange during a titration. Because the exchange rate k_{ex} (= $[B]k_{on} + k_{off}$) becomes faster with the increasing total ligand concentration $[B]_0$ titrated into the protein solution, the exchange regime might vary during the titration. If the exchange regime of the interaction becomes intermediate or slow-to-intermediate at a certain value of $[B]_0$, an observable

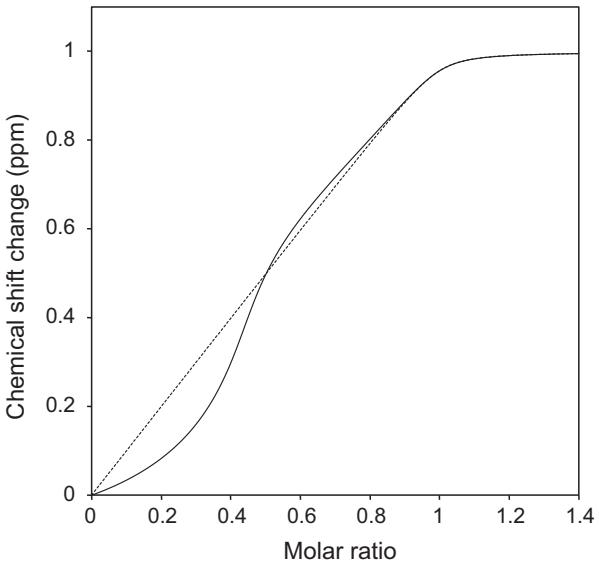

Fig. 3. Example of chemical shift titration for a two-state exchange model. The solid and dotted lines were calculated by using the McConnell equation and Eq. (17), respectively. The calculations used $\Delta\delta_{max}$ = 1 ppm, B_0 = 500 MHz, k_{on} = 10^9 M s^{-1}, k_{off} = 2000 s^{-1}, K_D = 2 μM, and $[A]_0$ = 1 mM. Under these conditions, $\Delta\omega$ is always 3141 rad s^{-1} during the titration, but k_{ex} increases with $[B]_0$ (Eqs. (2) and (3)). For example, k_{ex} is 2105 s^{-1} when $[B]_0$ is 0.05 mM ($k_{ex} < \Delta\omega$) and k_{ex} is 45733 s^{-1} when $[B]_0$ is 1 mM ($k_{ex} > \Delta\omega$).

NMR signal of each spin will not appear at the population-averaged chemical shifts of the free and bound states or even at the chemical shift of the free or bound states. This change in the exchange regime during a titration causes sigmoidal curvature of the chemical shift changes, and the titration data must be analyzed by the Bloch-McConnell equation [59,60].

Kovrigin [61] computationally explored the chemical-shift titration patterns of various interaction systems including three-state exchange models using the Bloch-McConnell equation [59,61]. Interestingly, for some three-state exchange systems that comprise a mixture of fast and slow transitions, one NMR signal (e.g., bound resonance) exhibits a gradual shift of its position similar to fast exchange and the other NMR signal (free resonance) becomes weaker without changing its position as the ligand concentration increases similar to slow exchange. Mittag et al. [62] showed experimentally by using line shape analysis of the titration data that the interaction between the N-terminal src homology 2 domain of phosphatidylinositide-3-kinase and ligand peptide includes an intermediate state and the exchange system comprises a mixture of fast and slow exchange.

4. Protein–ligand interactions in the intermediate- or slow-exchange regimes

When a protein–ligand interaction is in the intermediate- or slow-exchange regime, NMR quantities are not observed as population averages of the values in the free and bound states. NMR methods that are conducted under the assumption of population averaging due to fast exchange, such as chemical shift titration, transferred R_1, and transferred R_2 experiments, cannot be applied to an intermediate- or slow-exchange interaction. In the chemical-shift titration experiment, for example, NMR signals of a protein or ligand do not move during a titration for a system in slow exchange, or for systems in intermediate exchange they may disappear at certain protein–ligand concentration ratios. Thus, a titration curve suitable for deriving the dissociation constant cannot be drawn for either case. However, Latham et al. [28] determined the K_D value of the slow-exchange interaction between an RNA aptamer and the bronchodilator drug theophylline from a titration experiment. They measured the signal intensities of the free and the RNA–ligand complex resonances and estimated the bound fraction f_B, which varies according to the total concentrations of the RNA and drug in the NMR samples. Subsequently, the K_D value was calculated by replacing $\Delta\delta_{obs}$ in Eq. (17) with f_B, and fitting the data to this modified equation. This simple method, however, is applicable only to cases where the transverse relaxation rate R_2 of the bound state is either comparable to that of the free state or known a priori; otherwise, the fraction of the bound state might be underestimated because bound resonances relax faster than free resonances.

On the other hand, NMR methods that are designed to determine kinetic rates of intermediate- and slow-exchange systems, including protein–ligand interactions, have been developed, including R_2 dispersion [24–26,63,64], $R_{1\rho}$ dispersion [65,66], ZZ-exchange [27,67,68], chemical exchange saturation transfer (CEST) [69,70], and DEST [71]. These methods can be used to derive kinetic rates even though one of the states is not directly observable by NMR because of its low population and an excess relaxation rate, R_{ex}. For protein–ligand interactions, $[B]k_{on}$ and k_{off} can be determined in the same way used to determine the kinetic rates of conformational exchange in a single molecule. Extracting k_{on} from $[B]k_{on}$ is difficult, however, because [B] is also an unknown parameter that must be determined. In a typical sample for an interaction study using the above-listed NMR methods, the total concentration of B barely exceeds that of A, or does not exceed it at all. Therefore, only a very small fraction of B exists in the free state, making [B] difficult to determine experimentally. Demers and Mittermaier [72] determined K_D using ITC, and then calculated k_{on} according to $K_D = k_{off}/k_{on}$ using k_{off} determined by NMR. As an alternative, methods based on R_2 dispersion or ZZ-exchange spectroscopy have been developed to determine k_{on} and k_{off} with no previous information on K_D. In the following sections, we describe the theoretical and practical aspects of these R_2 dispersion and ZZ-exchange methods.

4.1. R_2 relaxation dispersion

R_2 relaxation dispersion spectroscopy is a transverse relaxation R_2 experiment that can quantitate site-specific kinetic rates on the millisecond timescale, the population of each interconverting state, and chemical-shift differences between the states. A unique property of R_2 dispersion is that it can probe low-populated minor states that are invisible to most biophysical methods. R_2 dispersion has been used for dynamics studies of a multitude of proteins, such as enzymes [73–79], intrinsically disordered proteins [29–31,80], antibodies [81,82], human leukocyte antigen [83], and transcriptional activators [84]. Recently, R_2 dispersion was even used to characterize the interaction between a ^{15}N-labeled small compound and an RNA aptamer [85].

Using R_2 dispersion, a method was developed to determine k_{on} and k_{off} rates with no previous information on K_D [31]. Under the condition that the exchange of an association–dissociation process in equilibrium takes place on the millisecond timescale accompanied by relatively large chemical-shift changes, the effective relaxation rate R_2^{eff} of both the free and bound resonances increases by an excess relaxation rate, R_{ex}. Analysis of R_2^{eff} by the R_2 dispersion experiment provides the exchange rate of the association–dissociation process k_{ex}, together with other parameters such as the chemical shift difference $\Delta\omega$ between the free and bound states. For the two-state exchange model (Eq. (1)), R_2^{eff} is calculated via the equation derived by Carver and Richards [86]:

$$R_2^{\mathrm{eff}} = R_{20} + \tfrac{1}{2}\{k_{\mathrm{ex}} - \tfrac{1}{\tau_{\mathrm{cp}}}\cosh^{-1}[D_+\cosh(\eta_+) - D_-\cos(\eta_-)]\}$$
$$D_\pm = \tfrac{1}{2}\left[\pm 1 + \frac{\Psi + 2\Delta\omega^2}{\sqrt{\Psi^2 + \xi^2}}\right]$$
$$\eta_\pm = \tau_{\mathrm{cp}}\sqrt{\tfrac{1}{2}\left(\pm\Psi + \sqrt{\Psi^2 + \xi^2}\right)} \qquad (18)$$
$$\Psi = k_{\mathrm{ex}}^2 - \Delta\omega^2$$
$$\xi = 2\Delta\omega([\mathrm{B}]k_{\mathrm{on}} - k_{\mathrm{off}})$$
$$k_{\mathrm{ex}} = [\mathrm{B}]k_{\mathrm{on}} + k_{\mathrm{off}}$$

where R_{20} denotes the intrinsic relaxation rate, which is usually assumed to be identical for the free and bound resonances. τ_{CP} denotes the delay between two successive 180° pulses in the Carr-Purcell-Meiboom-Gill pulse train. R_2^{eff} can also be calculated numerically via the Bloch-McConnell equation [59,87]. Provided that the protein–ligand interaction of interest is in the intermediate- or slow-exchange regime, k_{ex} can be separated into $[\mathrm{B}]k_{\mathrm{on}}$ and k_{off}; in the fast-exchange regime, however, only k_{ex}, $p_{\mathrm{A}}p_{\mathrm{B}}\Delta\omega^2$, and R_{20} can be determined by R_2 dispersion curve fitting.

As mentioned above, it is difficult to separate [B] and k_{on} from $[\mathrm{B}]k_{\mathrm{on}}$. Because Eq. (18) together with Eq. (2) indicates that k_{ex} depends on $[\mathrm{A}]_0$ and $[\mathrm{B}]_0$, k_{on} can be derived from a global fit of R_2 dispersion profiles measured for multiple samples with different $[\mathrm{A}]_0$ and $[\mathrm{B}]_0$. In practice, $[\mathrm{A}]_0$ (an isotope-labeled protein) is kept constant for a series of samples in order to measure R_2 dispersion spectra at similar sensitivity, and $[\mathrm{B}]_0$ (an unlabeled target molecule) is varied. Thus, Eq. (2) is modified for the fitting of R_2 dispersion profiles measured at multiple concentration ratios:

$$[\mathrm{B}] = \frac{1}{2}\left\{-K_{\mathrm{D}} - [\mathrm{A}]_0 + a[\mathrm{B}]_0 + \sqrt{(K_{\mathrm{D}} + [\mathrm{A}]_0 - a[\mathrm{B}]_0)^2 + 4a[\mathrm{B}]_0K_{\mathrm{D}}}\right\} \qquad (19)$$

where a denotes a ratio against a representative $[\mathrm{B}]_0$ value when $a = 1$, and is treated as an constant input parameter of the fitting for each NMR sample. Note that the experimentally determined concentrations $[\mathrm{A}]_0$ and $[\mathrm{B}]_0$ may contain some degree of error due to the experimental manipulations, which may in turn result in miscalculation of [B] and, of course, the fitting parameters such as k_{on} and k_{off}. For example, when $K_{\mathrm{D}} = 1$ μM, $[\mathrm{A}]_0 = 1$ mM, and $[\mathrm{B}]_0 = 1$ mM, [B] is calculated to be 31.1 μM. If $[\mathrm{B}]_0$ is wrongly determined to be 0.95 mM, corresponding to a 5% underestimation, [B] becomes 14.5 μM, which is 0.466 times smaller than the correct value. To accurately determine the parameters by curve fitting, therefore, it is necessary to include the concentrations $[\mathrm{A}]_0$ and $[\mathrm{B}]_0$ in the variable fitting parameters. It should also be noted that NMR samples for the R_2 dispersion experiments should be prepared carefully from a single concentrated stock solution of each molecule that has been dialyzed against the same buffer to render the concentration ratios accurate.

This R_2 dispersion method was first applied to an intrinsically disordered protein—the phosphorylated kinase-inducible domain (pKID) of the transcription factor CREB, which binds to the KIX domain of CREB-binding protein (CBP) [31]. In that study, R_2 dispersions of [^{15}N]-pKID were measured for samples with the KIX/pKID concentration ratios of 0.95, 1.00, 1.05, and 1.10 at the magnetic fields of 11.7 and 18.8 T. The measured R_2 dispersions were concentration-dependent and the amplitude of R_{ex} decreased with the concentration of KIX (Fig. 4) because the population of the minor state (encounter complex) decreased with the concentration of KIX. The R_2 dispersion curves at all four concentration ratios and at the two magnetic fields were fitted globally to the induced fit model (Eq. (6)), in which the chemical-shift differences $\Delta\omega$ were treated as global parameters for each residue and the folding and unfolding rates k_1 and k_{-1} were treated as global parameters for all residues in the cluster (neighboring residues within a local element of secondary structure). This analysis provided site-specific K_{D} values for pKID, and the mean K_{D} value was in excellent agreement the macroscopic K_{D} determined by ITC [88]. Together with chemical-shift titration experiments, the R_2 dispersion experiments revealed that pKID forms encounter complexes via non-specific interactions while it is unfolded, and evolves via a partially folded binding intermediate to the fully folded bound state. Thus, the pKID–KIX interaction can be explained by a linear four-state exchange model, comprising the free, encounter complex, folding intermediate and bound states. In the analysis, however, this interaction was treated as a pseudo four-state exchange (a three-state exchange equivalent to the induced fit) under the assumption that the exchange between the free state and the encounter complex is too fast to be detected by R_2 dispersion.

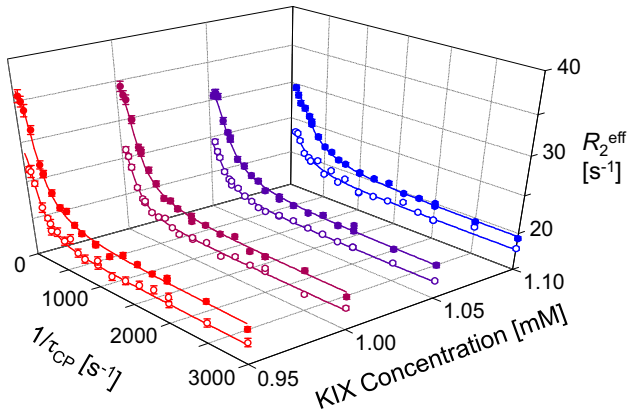

Fig. 4. R_2 dispersion profiles for Arg124 in pKID. R_2 dispersion data were recorded at 800 MHz (filled circles) and 500 MHz (open circles) for 1 mM ^{15}N-pKID in the presence of 0.95, 1.00, 1.05 and 1.10 mM KIX. Reproduced with permission from [31]. The global fit of the R_2 dispersion profiles provided k_{on}, k_{off}, k_1, k_{-1}, K_{D} in Eq. (6), and chemical shift differences between the encounter complex and bound state and between the encounter complex and intermediate state.

Recently, the same R_2 dispersion method was applied to the transactivation domain of the transcription factor c-Myb, which is another KIX-binding intrinsically disordered protein [29]. The findings revealed that the N-terminal region of c-Myb binds to KIX in a predominantly folded conformation, whereas the C-terminal region folds via an induced-fit process after binding to KIX.

The same authors further developed the R_2 dispersion method in order to determine k_{on}, k_{off}, and K_{D} without observable bound resonances in systems where the population of the bound state is very low [30]. As mentioned above, association–dissociation processes that occur on the millisecond timescale with relatively large chemical shift changes influence the R_2 relaxation rates of not only the bound but also the free resonances. Therefore, k_{on} and k_{off} can also be derived by analyzing R_2 dispersion curves of free resonances measured for multiple samples containing an isotope-labeled protein and sub-stoichiometric amounts of the target molecule at different concentration ratios. For such samples, bound resonances are unobservable because of the low population and line broadening caused by chemical exchange. The bound state is therefore probed as a minor state by the analysis of R_2 dispersion profiles.

This method was used to derive the k_{on}, k_{off}, and K_{D} values of the interaction between an intrinsically disordered protein, Asn803-hydroxylated hypoxia-inducible factor-1 (HIF-OH), and the transcriptional adapter zinc-binding (TAZ1) domain of CBP [30]. The HIF-OH concentration was kept at 510 μM, whereas the TAZ1 concentration was varied at 26.9, 21.5, 16.1, or 10.8 μM. The R_2 dispersion profiles obtained were concentration-dependent, and the amplitude of R_{ex} was found to increase with the concentration of

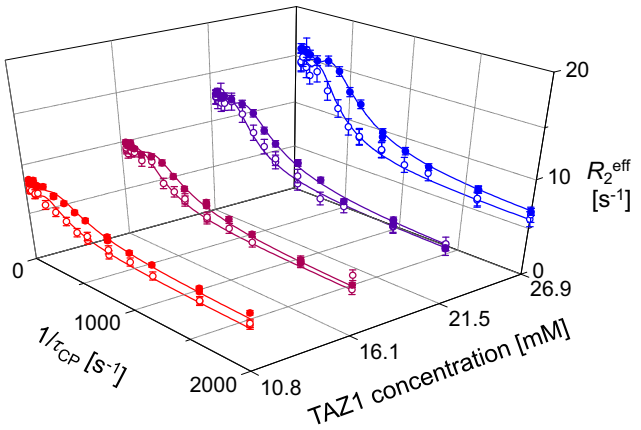

Fig. 5. R_2 dispersion profiles for Glu817 in HIF-OH. R_2 dispersion data were recorded at 900 MHz (filled circles) and 600 MHz (open circles) for 510 μM ^{15}N-HIF-OH in the presence of 10.8, 16.1, 21.5 and 26.9 μM TAZ1. Reproduced with permission from [30]. The global fit of the R_2 dispersion profiles provided k_{on}, k_{off}, K_D in Eq. (1), and chemical shift difference between the free and bound states.

TAZ1 (Fig. 5) because the population of the minor state (the bound state in this case) increased with the concentration of TAZ1. Again, the derived K_D value was in excellent agreement with the macroscopic K_D determined by ITC. The chemical shift differences between the free and bound states $\Delta\omega$ also agreed well with those calculated from the directly measured chemical shifts of the free and bound states.

For the bound state of TAZ1, the R_2 dispersion profiles were almost flat lines ($R_{ex} \approx 0\ s^{-1}$) because the exchange rate k_{ex} (= [TAZ1]k_{on} + k_{off}) was too fast owing to its very large k_{on} ($1.29 \times 10^9\ M^{-1}\ s^{-1}$) and the high concentration of [TAZ1], as compared with the chemical shift difference between the free and bound states. The association rate, [TAZ1]k_{on}, is the only parameter that directly depends on the concentration ratio; thus, it is the key factor that determines the amplitude of R_{ex}. In other words, it is important to optimize the concentration ratio to obtain good R_2 dispersion curves with a sufficient amplitude of R_{ex}. When k_{on} is very fast, R_2 dispersions should be measured for the free state of a protein in the presence of sub-stoichiometric amounts of the target molecule. Furthermore, in the relatively common case that bound resonances are unobservable owing to intermediate exchange, relaxation dispersion measurements for free ligand resonances might provide chemical shifts of the bound state and hence valuable structural information on the complex.

To the best of our knowledge, this R_2 dispersion method has not been applied to more complicated binding models. It is possible to calculate the concentration of free ligand numerically in more complicated models; however, it is not straightforward to determine accurate kinetic rate constants and chemical-shift differences by R_2 dispersion curve fitting because there are numerous adjustable parameters, implying that a variety of parameter sets have a comparable quality of fit. A multitude of R_2 dispersion data collected under different conditions, including concentration ratios, temperatures, magnetic field, and spin coherence, may be required to obtain the correct parameter set. For complicated exchange systems, it is more practical to analyze R_2 dispersion data in combination with other NMR methods and/or biochemical manipulation of the protein. Indeed, four- and five-exchange systems have been characterized by such strategies (see Refs. [89–91]).

In contrast to this approach, Hansen et al. [38] developed a unique method based on R_2 dispersion, which enabled the determination of k_{on}, k_{off}, and K_D of the interaction between histone chaperone Chz1 and variant histone H2A.Z-H2B. They used a single NMR sample with a concentration ratio very close to 1:1. The affinity of the complex was relatively high (K_D = ~0.2 μM), and thus both proteins were largely in the bound state with a small fraction in the free state. The unique strategy to derive k_{on} from a single sample was to uniformly label both Chz1 and H2A.Z-H2B with ^{2}H,^{15}N. The relaxation dispersions of both proteins were simultaneously measured, and the minor populations and the exchange rates of both proteins were independently estimated ([p_A, $k_{ex,A}$] and [p_B, $k_{ex,B}$]) by curve fitting each set of relaxation dispersions. The K_D and k_{off} values were calculated by the following equations:

$$K_D = \frac{[A][B]}{[A:B]} = \frac{p_A p_B [A:B]}{(1-p_A)(1-p_B)} \approx p_A p_B [A]_0 \quad (20)$$

$$k_{off} = (k_{ex,A} + k_{ex,B}) \frac{p_A p_B}{p_A + p_B} \quad (21)$$

where A and B (including the subscripts) correspond to Chz1 and H2A.Z-H2B, respectively. Ultimately, k_{on} was calculated as $k_{on} = k_{off}/K_D$.

4.2. ZZ-exchange

ZZ-exchange spectroscopy is a longitudinal relaxation technique to determine the auto-relaxation rates of two interconverting states that exchange on the millisecond to sub-second timescale [27]. This NMR method has been used to analyze the internal motions of proteins and binding kinetics of both protein–protein and protein–DNA interactions in the slow-exchange regime [32,67,68,92,93]. To quantitate binding kinetics by ZZ-exchange, the longitudinal relaxation profiles of the free and bound states and the two exchange peaks (i.e., free → bound and bound → free) of an isotope-labeled protein are analyzed simultaneously. It is essential to observe the free and bound resonances at the same time with signal intensities that are sufficiently high to allow the quantitation of auto-relaxation rates and exchange rates. For example, the sample would need to contain a half-stoichiometric amount of the target molecule.

Compared with R_2 dispersion spectroscopy, ZZ-exchange spectroscopy has two unique properties that are important for characterizing binding kinetics. First, ZZ-exchange is more sensitive to slower molecular motions as compared with R_2 dispersion. Because the longitudinal relaxation rates of proteins are usually slower than the transverse relaxation rates, slow molecular motions can perturb longitudinal magnetizations for longer during experimental relaxation delays. Second, ZZ-exchange does not require large chemical shift changes induced by binding to the target molecule because the longitudinal relaxation process is not affected by chemical shifts. In practice, free and bound resonances should be isolated sufficiently without peak overlap to quantitate their signal intensities. In contrast, R_2 dispersion requires large chemical shift changes upon binding to the target molecule. In this regard, application of R_2 dispersion is limited to flexible peptides or flexible regions of proteins, such as intrinsically disordered proteins, whereas ZZ-exchange can be used to quantitate the slow binding kinetics of a rigid protein whose chemical shifts (conformations) typically change little upon binding to the target molecule.

On the basis of these two properties of ZZ-exchange spectroscopy, Sugase developed a method to elucidate the slow binding events of a rigid protein, especially in cases where bound resonances are unobservable [37]. The concept of this approach is similar to that of the R_2 dispersion method applied to HIF-OH/TAZ1, as described above. In the following explanation, we assume that there is no internal slow conformational rearrangement affecting the ZZ-exchange profile. ZZ-exchange spectroscopy is usually not applicable to cases where bound resonances are unobservable but, similar to R_2 dispersion profiles, ZZ-exchange profiles of free resonances are modified by the association–dissociation process in a concentration-dependent manner as shown by Eq. (22) [27] for a two-state exchange model (Eq. (1)):

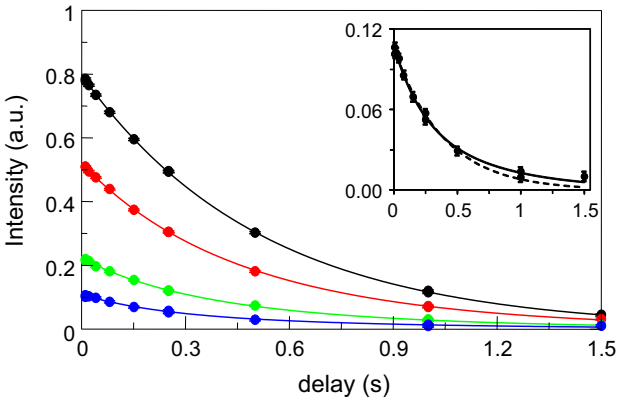

Fig. 6. ZZ-exchange profiles for Thr11 in GB1. ZZ-exchange data were recorded at GB1:IgG concentration ratios of 1:0 (black), 1:0.1 (red), 1:0.2 (green), and 1:0.3 (blue). The global fit of the ZZ-exchange profiles provided k_{on}, k_{off}, K_D in Eq. (1). The inset is a close-up view of the profiles for the 1:0.3 sample fitted with Eq. (22) (solid line) and Eq. (23) (dashed line). Reproduced with permission from [37].

$$I_F(t) = \frac{I_F(0)}{\lambda_+ - \lambda_-}[(\lambda_+ - R_{1F} - [B]k_{on})\exp(-\lambda_- t) - (\lambda_- - R_{1F} - [B]k_{on})\exp(-\lambda_+ t)]$$
$$\lambda_\pm = \frac{1}{2}\left[R_{1F} + R_{1B} + [B]k_{on} + k_{off} \pm \sqrt{(R_{1F} - R_{1B} + [B]k_{on} - k_{off})^2 + 4[B]k_{on}k_{off}}\right] \quad (22)$$

where R_{1F} and R_{1B} denote the auto-relaxation rates of the ligand in the free and bound states, respectively. Similar to the R_2 dispersion method, [B] is calculated by Eq. (19), and it is also necessary to include the concentrations $[A]_0$ and $[B]_0$ in the fitting parameters. When $[B]_0$ is zero, corresponding to the situation that A is completely in the free state, Eq. (22) can be simplified as:

$$I_F(t) = I_F(0)\exp(-R_{1F}t) \quad (23)$$

The curve drawn by this equation is identical to the longitudinal relaxation profile measured in the regular R_1 relaxation experiment. Therefore, the auto-relaxation rate of the free state R_{1F} in Eq. (22) can be independently determined.

The ZZ-exchange method is similar to the transferred R_1 experiment described above; however, the application of the transferred R_1 experiment is limited to the condition of fast exchange. A major difference between this ZZ-exchange method and the transferred R_1 method is their mathematical treatments for determining the dissociation constant from relaxation profiles. In ZZ-exchange, the dissociation constant is calculated from the binding kinetics k_{on} and k_{off} ($K_D = k_{off}/k_{on}$). In transferred R_1, by contrast, the R_1 relaxation rate is measured as a population-averaged value of the free and bound states of a ligand (Eq. (15)). The difference between R_{1F} and R_{1B} should be large enough to quantitate p_B accurately for the transferred R_1 method using Eq. (15). From another viewpoint, Eq. (16) indicates that the transferred R_1 method cannot determine k_{on} and k_{off} rates. In contrast, the ZZ-exchange method is applicable even in the case where the difference R_{1F} and R_{1B} is small if $[B]k_{on}$ and k_{off} perturb the ZZ-exchange profile, which is defined by $[B]k_{on}$ and k_{off}, as well as R_{1F} and R_{1B} (Eq. (22)).

Sugase applied the ZZ-exchange method to interaction between the B1 domain of *Streptococcus* protein G (GB1), a rigid globular protein composed of 56 residues, and immunoglobulin G (IgG) [37]. Previous structural studies indicated that GB1 binds to each of the two heavy chains in the Fc region of IgG with little conformational change [94,95]. The binding kinetics of this interaction could not be analyzed by the R_2 dispersion method described above. In the ZZ-exchange experiment, the GB1 concentration was kept at 200 μM, whereas the IgG concentration was varied at 0, 20, 40, or 60 μM. The ZZ-exchange profiles obtained were concentration-dependent (Fig. 6). The inset shows that later points deviate more from the theoretical curve calculated with Eq. (23) (the regular R_1 experiment) than from that calculated with Eq. (22) (the ZZ-exchange experiment). The ZZ-exchange experiments enabled us to determine k_{on} (1.50×10^7 M^{-1} s^{-1}), k_{off} (2.23 s^{-1}), and consequently, K_D (149 nM).

5. Conclusion

We described that NMR is a very powerful tool to analyze protein–ligand interactions quantitatively. There are various NMR methods, and it is essential to choose one that is appropriate for analyzing the protein–ligand interaction of interest. In particular, the exchange regime of the interaction is one of the most important factors in selecting an appropriate method. Even for a simple chemical shift titration experiment, the simplest equation (Eq. (17)) for determining K_D from the chemical shift data is not always valid.

The recent advent of new relaxation experiments has enabled us to characterize slower protein–ligand interactions in detail. Such relaxation experiments provide kinetic information on interactions but, again, it is critical to choose an appropriate kinetic model, such as a two- or three-state exchange model, to derive correct kinetic information. How can we validate whether the chosen model is appropriate? There is no general rule, but it must be confirmed, at least, that the parameters obtained are physiologically reasonable and consistent with previous data, and the fitting quality of a certain model is statistically better than that of other models. For example, if the k_{on} obtained is more than 10^{10} M^{-1} s^{-1}, the chosen model might be inappropriate, whereas if the K_D obtained is comparable to that determined by another method, the chosen model is likely to be appropriate. In terms of comparing the fitting quality, the *F*-test and Akaike's information criterion are often used [96].

We have also described two recent types of NMR method that utilize R_2 dispersion or ZZ-exchange. Both methods can determine the binding kinetics and dissociation constant. Essential steps in both methods are the careful preparation of multiple NMR samples with different concentration ratios and global data analysis using an appropriate kinetic model [39]. Because the pulse programs were not modified, it would be easy to extend these methods to larger protein–ligand interactions by adopting TROSY-type measurements [63,64,67,68]. It should also be possible to develop similar methods using other NMR measurements such as CEST [69,70], DEST [71], or $R_{1\rho}$ dispersion [65,66], or other spin types of R_2 dispersion [97–102].

NMR has firmly established its position in studies of protein–ligand interactions. Furthermore, new NMR methods are still being developed to analyze difficult protein–ligand interactions and to obtain more detailed insight into them. As a result, NMR will remain central to such studies or even elevate its position in future research.

Acknowledgements

This work was supported by funding from Suntory Holdings, a Grant-in-Aid for Scientific Research on Innovative Areas, and a Grant-in-Aid for Scientific Research (B) from MEXT, Japan, for K. S.; a Grant-in-Aid for Young Scientists (B) from MEXT, Japan, for A.F. and T.K.; and a Grant-in-Aid for JSPS Fellows from MEXT, Japan, for S.Y.

References

[1] K.K. Frederick, M.S. Marlow, K.G. Valentine, A.J. Wand, Conformational entropy in molecular recognition by proteins, Nature 448 (2007) 325–329.
[2] R.E. Babine, S.L. Bender, Molecular recognition of protein–ligand complexes: applications to drug design, Chem. Rev. 97 (1997) 1359–1472.

[3] E. Lionta, G. Spyrou, D.K. Vassilatis, Z. Cournia, Structure-based virtual screening for drug discovery: principles, applications and recent advances, Curr. Top. Med. Chem. 14 (2014) 1923–1938.
[4] O.C. Redfern, B. Dessailly, C.A. Orengo, Exploring the structure and function paradigm, Curr. Opin. Struct. Biol. 18 (2008) 394–402.
[5] M. Karplus, J. Kuriyan, Molecular dynamics and protein function, Proc. Natl. Acad. Sci. USA 102 (2005) 6679–6685.
[6] M. Karplus, Dynamical aspects of molecular recognition, J. Mol. Recognit.: JMR 23 (2010) 102–104.
[7] P. Fechner, O. Bleher, M. Ewald, K. Freudenberger, D. Furin, U. Hilbig, F. Kolarov, K. Krieg, L. Leidner, G. Markovic, G. Proll, F. Proll, S. Rau, J. Riedt, B. Schwarz, P. Weber, J. Widmaier, Size does matter! Label-free detection of small molecule–protein interaction, Anal. Bioanal. Chem. 406 (2014) 4033–4051.
[8] K. Nienhaus, G.U. Nienhaus, Probing heme protein–ligand interactions by UV/visible absorption spectroscopy, Methods Mol. Biol. 305 (2005) 215–242.
[9] S.E. Harding, A.J. Rowe, Insight into protein–protein interactions from analytical ultracentrifugation, Biochem. Soc. Trans. 38 (2010) 901–907.
[10] F. Zsila, Z. Bikadi, I. Fitos, M. Simonyi, Probing protein binding sites by circular dichroism spectroscopy, Curr. Drug Discov. Technol. 1 (2004) 133–153.
[11] B.D. Slaughter, R. Li, Toward quantitative "in vivo biochemistry" with fluorescence fluctuation spectroscopy, Mol. Biol. Cell 21 (2010) 4306–4311.
[12] F.H. Niesen, H. Berglund, M. Vedadi, The use of differential scanning fluorimetry to detect ligand interactions that promote protein stability, Nat. Protoc. 2 (2007) 2212–2221.
[13] C.J. Fee, Label-free, real-time interaction and adsorption analysis 1: surface plasmon resonance, Methods Mol. Biol. 996 (2013) 287–312.
[14] M. Kabiri, L.D. Unsworth, Application of isothermal titration calorimetry for characterizing thermodynamic parameters of biomolecular interactions: peptide self-assembly and protein adsorption case studies, Biomacromolecules 15 (2014) 3463–3473.
[15] C.J. Fee, Label-free, real-time interaction and adsorption analysis 2: quartz crystal microbalance, Methods Mol. Biol. 996 (2013) 313–322.
[16] J. Kool, N. Jonker, H. Irth, W.M. Niessen, Studying protein–protein affinity and immobilized ligand–protein affinity interactions using MS-based methods, Anal. Bioanal. Chem. 401 (2011) 1109–1125.
[17] J.J. Perry, J.A. Tainer, Developing advanced X-ray scattering methods combined with crystallography and computation, Methods 59 (2013) 363–371.
[18] A.M. Whited, P.S. Park, Atomic force microscopy: a multifaceted tool to study membrane proteins and their interactions with ligands, Biochim. Biophys. Acta 2014 (1838) 56–68.
[19] K. Takeuchi, G. Wagner, NMR studies of protein interactions, Curr. Opin. Struct. Biol. 16 (2006) 109–117.
[20] L. Fielding, S. Rutherford, D. Fletcher, Determination of protein–ligand binding affinity by NMR: observations from serum albumin model systems, Magn. Reson. Chem.: MRC 43 (2005) 463–470.
[21] L. Fielding, NMR methods for the determination of protein–ligand dissociation constants, Prog. Nucl. Magn. Reson. Spectrosc. 51 (2007) 219–242.
[22] A.J. Rowe, Ultra-weak reversible protein–protein interactions, Methods 54 (2011) 157–166.
[23] M.P. Williamson, Using chemical shift perturbation to characterise ligand binding, Prog. Nucl. Magn. Reson. Spectrosc. 73 (2013) 1–16.
[24] J.P. Loria, M. Rance, A.G. Palmer, A relaxation-compensated Carr-Purcell-Meiboom-Gill sequence for characterizing chemical exchange by NMR spectroscopy, J. Am. Chem. Soc. 121 (1999) 2331–2332.
[25] M. Tollinger, N.R. Skrynnikov, F.A. Mulder, J.D. Forman-Kay, L.E. Kay, Slow dynamics in folded and unfolded states of an SH3 domain, J. Am. Chem. Soc. 123 (2001) 11341–11352.
[26] D.F. Hansen, P. Vallurupalli, L.E. Kay, An improved ^{15}N relaxation dispersion experiment for the measurement of millisecond time-scale dynamics in proteins†, J. Phys. Chem. B 112 (2008) 5898–5904.
[27] N.A. Farrow, O. Zhang, J.D. Forman-Kay, L.E. Kay, A heteronuclear correlation experiment for simultaneous determination of ^{15}N longitudinal decay and chemical exchange rates of systems in slow equilibrium, J. Biomol. NMR 4 (1994) 727–734.
[28] M.P. Latham, G.R. Zimmermann, A. Pardi, NMR chemical exchange as a probe for ligand-binding kinetics in a theophylline-binding RNA aptamer, J. Am. Chem. Soc. 131 (2009) 5052–5053.
[29] M. Arai, K. Sugase, H.J. Dyson, P.E. Wright, Conformational propensities of intrinsically disordered proteins influence the mechanism of binding and folding, Proc. Natl. Acad. Sci. USA 112 (2015) 9614–9619.
[30] K. Sugase, J.C. Lansing, H.J. Dyson, P.E. Wright, Tailoring relaxation dispersion experiments for fast-associating protein complexes, J. Am. Chem. Soc. 129 (2007) 13406–13407.
[31] K. Sugase, H.J. Dyson, P.E. Wright, Mechanism of coupled folding and binding of an intrinsically disordered protein, Nature 447 (2007) 1021–1025.
[32] Y. Li, N.L. Altorelli, F. Bahna, B. Honig, L. Shapiro, A.G. Palmer 3rd, Mechanism of E-cadherin dimerization probed by NMR relaxation dispersion, Proc. Natl. Acad. Sci. USA 110 (2013) 16462–16467.
[33] P. Vallurupalli, D.F. Hansen, L.E. Kay, Structures of invisible, excited protein states by relaxation dispersion NMR spectroscopy, Proc. Natl. Acad. Sci. USA 105 (2008) 11766–11771.
[34] Y. Takayama, G.M. Clore, Interplay between minor and major groove-binding transcription factors Sox2 and Oct1 in translocation on DNA studied by paramagnetic and diamagnetic NMR, J. Biol. Chem. 287 (2012) 14349–14363.
[35] Y. Takayama, G.M. Clore, Impact of protein/protein interactions on global intermolecular translocation rates of the transcription factors Sox2 and Oct1 between DNA cognate sites analyzed by z-exchange NMR spectroscopy, J. Biol. Chem. 287 (2012) 26962–26970.
[36] C.J. Markin, L.F. Saltibus, M.J. Kean, R.T. McKay, W. Xiao, L. Spyracopoulos, Catalytic proficiency of ubiquitin conjugation enzymes: balancing pK(a) suppression, entropy, and electrostatics, J. Am. Chem. Soc. 132 (2010) 17775–17786.
[37] K. Sugase, Elucidating slow binding kinetics of a protein without observable bound resonances by longitudinal relaxation NMR spectroscopy, J. Biomol. NMR 50 (2011) 219–227.
[38] D.F. Hansen, Z. Zhou, H. Feng, L.M.M. Jenkins, Y. Bai, L.E. Kay, Binding kinetics of histone chaperone chz1 and variant histone H2A.Z-H2B by relaxation dispersion NMR spectroscopy, J. Mol. Biol. 387 (2009) 1–9.
[39] K. Sugase, T. Konuma, J.C. Lansing, P.E. Wright, Fast and accurate fitting of relaxation dispersion data using the flexible software package GLOVE, J. Biomol. NMR 56 (2013) 275–283.
[40] A. Furukawa, K. Sugase, R. Morishita, T. Nagata, T. Kodaki, A. Takaori-Kondo, A. Ryo, M. Katahira, Quantitative analysis of location- and sequence-dependent deamination by APOBEC3G using real-time NMR spectroscopy, Angew. Chem. 53 (2014) 2349–2352.
[41] M.J. Smith, C.B. Marshall, F.X. Theillet, A. Binolfi, P. Selenko, M. Ikura, Real-time NMR monitoring of biological activities in complex physiological environments, Curr. Opin. Struct. Biol. 32C (2015) 39–47.
[42] J. Cavanagh, W.J. Fairbrother, A.G. Palmer III, M. Rance, N.J. Skelton, Protein NMR Spectroscopy, Principles and Practice, second ed., Academic Press, 2006.
[43] D.E. Koshland, Application of a theory of enzyme specificity to protein synthesis, Proc. Natl. Acad. Sci. USA 44 (1958) 98–104.
[44] M. Eigen, Determination of general and specific ionic interactions in solution, Discuss. Faraday Soc. 24 (1957) 25.
[45] J. Angulo, P.M. Enriquez-Navas, P.M. Nieto, Ligand–receptor binding affinities from saturation transfer difference (STD) NMR spectroscopy: the binding isotherm of STD initial growth rates, Chemistry 16 (2010) 7803–7812.
[46] M. Mayer, B. Meyer, Characterization of ligand binding by saturation transfer difference NMR spectroscopy, Angew. Chem.-Int. Ed. 38 (1999) 1784–1788.
[47] C. Dalvit, P. Pevarello, M. Tato, M. Veronesi, A. Vulpetti, M. Sundstrom, Identification of compounds with binding affinity to proteins via magnetization transfer from bulk water, J. Biomol. NMR 18 (2000) 65–68.
[48] C. Dalvit, G. Fogliatto, A. Stewart, M. Veronesi, B. Stockman, WaterLOGSY as a method for primary NMR screening: practical aspects and range of applicability, J. Biomol. NMR 21 (2001) 349–359.
[49] S.R. LaPlante, N. Aubry, R. Déziel, F. Ni, P. Xu, Transferred 13CT1 relaxation at natural isotopic abundance: a practical method for determining site-specific changes in ligand flexibility upon binding to a macromolecule, J. Am. Chem. Soc. 122 (2000) 12530–12535.
[50] X.C. Su, S. Jergic, K. Ozawa, N.D. Burns, N.E. Dixon, G. Otting, Measurement of dissociation constants of high-molecular weight protein–protein complexes by transferred ^{15}N-relaxation, J. Biomol. NMR 38 (2007) 65–72.
[51] B. Meyer, T. Peters, NMR spectroscopy techniques for screening and identifying ligand binding to protein receptors, Angew. Chem. 42 (2003) 864–890.
[52] C. Dalvit, M. Fasolini, M. Flocco, S. Knapp, P. Pevarello, M. Veronesi, NMR-based screening with competition water-ligand observed via gradient spectroscopy experiments: detection of high-affinity ligands, J. Med. Chem. 45 (2002) 2610–2614.
[53] C. Ludwig, U.L. Guenther, Ligand based NMR methods for drug discovery, Front. Biosci. (Landmark Ed.) 14 (2009) 4565–4574.
[54] A. Antanasijevic, B. Ramirez, M. Caffrey, Comparison of the sensitivities of WaterLOGSY and saturation transfer difference NMR experiments, J. Biomol. NMR 60 (2014) 37–44.
[55] C.J. Markin, L. Spyracopoulos, Increased precision for analysis of protein–ligand dissociation constants determined from chemical shift titrations, J. Biomol. NMR 53 (2012) 125–138.
[56] C.J. Markin, L. Spyracopoulos, Accuracy and precision of protein–ligand interaction kinetics determined from chemical shift titrations, J. Biomol. NMR 54 (2012) 355–376.
[57] J.C. Ferreon, C.W. Lee, M. Arai, M.A. Martinez-Yamout, H.J. Dyson, P.E. Wright, Cooperative regulation of p53 by modulation of ternary complex formation with CBP/p300 and HDM2, Proc. Natl. Acad. Sci. USA 106 (2009) 6591–6596.
[58] M. Arai, H.J. Dyson, P.E. Wright, Leu628 of the KIX domain of CBP is a key residue for the interaction with the MLL transactivation domain, FEBS Lett. 584 (2010) 4500–4504.
[59] H.M. Mcconnell, Reaction rates by nuclear magnetic resonance, J. Chem. Phys. 28 (1958) 430–431.
[60] J. Feeney, J.G. Batchelor, J.P. Albrand, G.C.K. Roberts, Effects of intermediate exchange processes on the estimation of equilibrium-constants by NMR, J. Magn. Reson. 33 (1979) 519–529.
[61] E.L. Kovrigin, NMR line shapes and multi-state binding equilibria, J. Biomol. NMR 53 (2012) 257–270.
[62] T. Mittag, B. Schaffhausen, U.L. Gunther, Tracing kinetic intermediates during ligand binding, J. Am. Chem. Soc. 126 (2004) 9017–9023.

[63] J.P. Loria, M. Rance, A.G. Palmer 3rd, A TROSY CPMG sequence for characterizing chemical exchange in large proteins, J. Biomol. NMR 15 (1999) 151–155.
[64] P. Vallurupalli, D.F. Hansen, E. Stollar, E. Meirovitch, L.E. Kay, Measurement of bond vector orientations in invisible excited states of proteins, Proc. Natl. Acad. Sci. USA 104 (2007) 18473–18477.
[65] F. Massi, E. Johnson, C. Wang, M. Rance, A.G. Palmer 3rd, NMR R1 rho rotating-frame relaxation with weak radio frequency fields, J. Am. Chem. Soc. 126 (2004) 2247–2256.
[66] D.M. Korzhnev, V.Y. Orekhov, L.E. Kay, Off-resonance R1ρNMR studies of exchange dynamics in proteins with low spin-lock fields: an application to a Fyn SH3 domain, J. Am. Chem. Soc. 127 (2005) 713–721.
[67] D. Sahu, G.M. Clore, J. Iwahara, TROSY-based z-exchange spectroscopy: application to the determination of the activation energy for intermolecular protein translocation between specific sites on different DNA molecules, J. Am. Chem. Soc. 129 (2007) 13232–13237.
[68] Y. Li, A.G. Palmer 3rd, TROSY-selected ZZ-exchange experiment for characterizing slow chemical exchange in large proteins, J. Biomol. NMR 45 (2009) 357–360.
[69] P. Vallurupalli, G. Bouvignies, L.E. Kay, Studying "invisible" excited protein states in slow exchange with a major state conformation, J. Am. Chem. Soc. 134 (2012) 8148–8161.
[70] G. Bouvignies, L.E. Kay, A 2D (1)(3)C-CEST experiment for studying slowly exchanging protein systems using methyl probes: an application to protein folding, J. Biomol. NMR 53 (2012) 303–310.
[71] N.L. Fawzi, J. Ying, R. Ghirlando, D.A. Torchia, G.M. Clore, Atomic-resolution dynamics on the surface of amyloid-beta protofibrils probed by solution NMR, Nature 480 (2011) 268–272.
[72] J.P. Demers, A. Mittermaier, Binding mechanism of an SH3 domain studied by NMR and ITC, J. Am. Chem. Soc. 131 (2009) 4355–4367.
[73] D.D. Boehr, D. McElheny, H.J. Dyson, P.E. Wright, The dynamic energy landscape of dihydrofolate reductase catalysis, Science 313 (2006) 1638–1642.
[74] K.A. Henzler-Wildman, V. Thai, M. Lei, M. Ott, M. Wolf-Watz, T. Fenn, E. Pozharski, M.A. Wilson, G.A. Petsko, M. Karplus, C.G. Hubner, D. Kern, Intrinsic motions along an enzymatic reaction trajectory, Nature 450 (2007) 838–844.
[75] E.Z. Eisenmesser, O. Millet, W. Labeikovsky, D.M. Korzhnev, M. Wolf-Watz, D. A. Bosco, J.J. Skalicky, L.E. Kay, D. Kern, Intrinsic dynamics of an enzyme underlies catalysis, Nature 438 (2005) 117–121.
[76] S.K. Whittier, A.C. Hengge, J.P. Loria, Conformational motions regulate phosphoryl transfer in related protein tyrosine phosphatases, Science 341 (2013) 899–903.
[77] G. Bhabha, J. Lee, D.C. Ekiert, J. Gam, I.A. Wilson, H.J. Dyson, S.J. Benkovic, P.E. Wright, A dynamic knockout reveals that conformational fluctuations influence the chemical step of enzyme catalysis, Science 332 (2011) 234–238.
[78] E. Harada, M. Sugishima, J. Harada, K. Fukuyama, K. Sugase, Distal regulation of heme binding of heme oxygenase-1 mediated by conformational fluctuations, Biochemistry 54 (2015) 340–348.
[79] R. Sprangers, A. Gribun, P.M. Hwang, W.A. Houry, L.E. Kay, Quantitative NMR spectroscopy of supramolecular complexes: dynamic side pores in ClpP are important for product release, Proc. Natl. Acad. Sci. USA 102 (2005) 16678–16683.
[80] R. Schneider, D. Maurin, G. Communie, J. Kragelj, D.F. Hansen, R.W. Ruigrok, M.R. Jensen, M. Blackledge, Visualizing the molecular recognition trajectory of an intrinsically disordered protein using multinuclear relaxation dispersion NMR, J. Am. Chem. Soc. 137 (2015) 1220–1229.
[81] S. Mukherjee, S.P. Pondaven, C.P. Jaroniec, Conformational flexibility of a human immunoglobulin light chain variable domain by relaxation dispersion nuclear magnetic resonance spectroscopy: implications for protein misfolding and amyloid assembly, Biochemistry 50 (2011) 5845–5857.
[82] A.W. Barb, J.H. Prestegard, NMR analysis demonstrates immunoglobulin G N-glycans are accessible and dynamic, Nat. Chem. Biol. 7 (2011) 147–153.
[83] S. Yanaka, T. Ueno, Y. Shi, J. Qi, G.F. Gao, K. Tsumoto, K. Sugase, Peptide-dependent conformational fluctuation determines the stability of the human leukocyte antigen class I complex, J. Biol. Chem. 289 (2014) 24680–24690.
[84] S.R. Tzeng, C.G. Kalodimos, Dynamic activation of an allosteric regulatory protein, Nature 462 (2009) 368–372.
[85] T. Moschen, C.H. Wunderlich, R. Spitzer, J. Levic, R. Micura, M. Tollinger, C. Kreutz, Ligand-detected relaxation dispersion NMR spectroscopy: dynamics of preQ1-RNA binding, Angew. Chem. 54 (2015) 560–563.
[86] J.P. Carver, R.E. Richards, A general two-site solution for the chemical exchange produced dependence of T2 upon the carr-Purcell pulse separation, J. Magn. Reson. 6 (1972) (1969) 89–105.
[87] D.M. Korzhnev, X. Salvatella, M. Vendruscolo, A.A. Di Nardo, A.R. Davidson, C. M. Dobson, L.E. Kay, Low-populated folding intermediates of Fyn SH3 characterized by relaxation dispersion NMR, Nature 430 (2004) 586–590.
[88] N.K. Goto, T. Zor, M. Martinez-Yamout, H.J. Dyson, P.E. Wright, Cooperativity in transcription factor binding to the coactivator CREB-binding protein (CBP). The mixed lineage leukemia protein (MLL) activation domain binds to an allosteric site on the KIX domain, J. Biol. Chem. 277 (2002) 43168–43174.
[89] P. Li, I.R. Martins, M.K. Rosen, The feasibility of parameterizing four-state equilibria using relaxation dispersion measurements, J. Biomol. NMR 51 (2011) 57–70.
[90] D.S. Libich, V. Tugarinov, G.M. Clore, Intrinsic unfoldase/foldase activity of the chaperonin GroEL directly demonstrated using multinuclear relaxation-based NMR, Proc. Natl. Acad. Sci. USA 112 (2015) 8817–8823.
[91] A. Sekhar, J.A. Rumfeldt, H.R. Broom, C.M. Doyle, G. Bouvignies, E.M. Meiering, L.E. Kay, Thermal fluctuations of immature SOD1 lead to separate folding and misfolding pathways, eLife 4 (2015) e07296.
[92] T. Wauer, K.N. Swatek, J.L. Wagstaff, C. Gladkova, J.N. Pruneda, M.A. Michel, M. Gersch, C.M. Johnson, S.M. Freund, D. Komander, Ubiquitin Ser65 phosphorylation affects ubiquitin structure, chain assembly and hydrolysis, EMBO J. 34 (2015) 307–325.
[93] M. Doucleff, G.M. Clore, Global jumping and domain-specific intersegment transfer between DNA cognate sites of the multidomain transcription factor Oct-1, Proc. Natl. Acad. Sci. USA 105 (2008) 13871–13876.
[94] A.E. Sauer-Eriksson, G.J. Kleywegt, M. Uhlen, T.A. Jones, Crystal structure of the C2 fragment of streptococcal protein G in complex with the Fc domain of human IgG, Structure 3 (1995) 265–278.
[95] A.M. Gronenborn, D.R. Filpula, N.Z. Essig, A. Achari, M. Whitlow, P.T. Wingfield, G.M. Clore, A novel, highly stable fold of the immunoglobulin binding domain of streptococcal protein G, Science 253 (1991) 657–661.
[96] M. Harvey, A. Christopoulos, Fitting Models to Biological Data using Linear and Nonlinear Regression: A Practical Guide to Curve Fitting, Oxford University Press, 2004.
[97] V.Y. Orekhov, D.M. Korzhnev, L.E. Kay, Double- and zero-quantum NMR relaxation dispersion experiments sampling millisecond time scale dynamics in proteins, J. Am. Chem. Soc. 126 (2004) 1886–1891.
[98] P. Lundstrom, P. Vallurupalli, T.L. Religa, F.W. Dahlquist, L.E. Kay, A single-quantum methyl ^{13}C-relaxation dispersion experiment with improved sensitivity, J. Biomol. NMR 38 (2007) 79–88.
[99] D.F. Hansen, P. Vallurupalli, L.E. Kay, Quantifying two-bond 1HN–13CO and one-bond ^{1}H(alpha)–^{13}C(alpha) dipolar couplings of invisible protein states by spin-state selective relaxation dispersion NMR spectroscopy, J. Am. Chem. Soc. 130 (2008) 8397–8405.
[100] P. Lundstrom, D.F. Hansen, P. Vallurupalli, L.E. Kay, Accurate measurement of alpha proton chemical shifts of excited protein states by relaxation dispersion NMR spectroscopy, J. Am. Chem. Soc. 131 (2009) 1915–1926.
[101] P. Lundstrom, H. Lin, L.E. Kay, Measuring ^{13}C beta chemical shifts of invisible excited states in proteins by relaxation dispersion NMR spectroscopy, J. Biomol. NMR 44 (2009) 139–155.
[102] P. Vallurupalli, D.F. Hansen, P. Lundstrom, L.E. Kay, CPMG relaxation dispersion NMR experiments measuring glycine ^{1}H alpha and ^{13}C alpha chemical shifts in the 'invisible' excited states of proteins, J. Biomol. NMR 45 (2009) 45–55.

Glossary of abbreviations

CBP: CREB-binding protein
CEST: chemical exchange saturation transfer
DEST: dark-state exchange saturation transfer
GB1: the B1 domain of *Streptococcus* protein G
HIF-OH: hydroxylated hypoxia-inducible factor-1
IgG: immunoglobulin G
ITC: isothermal titration calorimetry
pKID: phosphorylated kinase-inducible domain
STD: saturation-transfer difference
TAZ1: transcriptional adapter zinc-binding
WaterLOGSY: water-ligand observed via gradient spectroscopy